CO Binding Trends on Model Me_1/Fe_3O_4 Single-Atom Catalysts

Jan Hulva,[1*] Matthias Meier,[1,2*] Roland Bliem,[1] Zdenek Jakub,[1] Michael Schmid,[1] Ulrike Diebold,[1] Cesare Franchini,[2] Gareth S. Parkinson[1#]

[1] Institute of Applied Physics, TU Wien, Vienna, Austria

[2] Computational Materials Physics, University of Vienna, Vienna, Austria

*These authors contributed equally to this work

Abstract

Understanding how the local environment of a "single-atom" catalyst affect stability and reactivity remains a significant challenge. Here, we present an in-depth study of Cu_1, Ag_1, Au_1, Ni_1, Pd_1, Pt_1, Rh_1, and Ir_1 species on $Fe_3O_4(001)$; a model support where all metals occupy the same 2-fold coordinated adsorption site upon deposition at room temperature. Using a combination of surface science techniques, we show that CO adsorption strength differs significantly from the respective metal surfaces and supported clusters. Charge transfer into the support modifies the d-states of the metal atom, and with it the strength of the metal-CO bond. The effect can go both ways depending on the metal, with the Ag-CO bond significantly stronger and Ni-CO significantly weaker. CO-induced structural distortions play a major role, reducing the adsorption energies significantly from that expected based on electronic structure alone. Overall, our results show how the properties of oxide-supported metal atoms depend sensitively on the coordination environment and local geometry, and that a new chemical intuition will be required to identify the best metal/support combinations for a particular reaction.

[#] Email: parkinson@iap.tuwien.ac.at

Main Text

The reactivity of oxide-supported metal nanoparticle catalysts has traditionally been understood using models developed for extended metal surfaces.[1] Such a picture does not seem reasonable for so-called "single-atom" catalysts (SACs),[2, 3, 4, 5, 6, 7, 8] because the isolated metal atoms are stabilized by chemical bonds to the support and are often charged. In this regard, SAC systems resemble coordination complexes, and there is much excitement at the prospect that SACs can be used to "heterogenize" problematic reactions currently performed in solution.[9, 10, 11] While there are similarities, there are also significant practical differences. Homogeneous catalysts are designed for purpose based on a fundamental understanding of the structure function-relationship, and the ligands play an important role activating reactants and stabilizing intermediates. Complexes containing O^{2-} ligands are rare,[5] and the binding environment of the metal adatom on the metal oxide is difficult to ascertain and control. Since robust, inexpensive metal oxides are set to continue as the support of choice in SAC, it is vital to learn how the coordination of the metal site on an oxide surface affect its charge state, and how this relates to its adsorption properties and ultimately catalytic activity.

Most studies of oxide-supported SACs feature transmission electron microscopy (TEM) images[12] of powder samples showing that the metal adatoms align with the cationic sublattice. This fits with x-ray absorption near edge structure (XANES) spectra, which typically suggest coordination to oxygen. Density functional theory (DFT) calculations,[13, 14, 15, 16] also predict such sites to be most stable (albeit on simplified models of the support surface). A positive charge state can be inferred from x-ray photoelectron spectroscopy (XPS) and/or infrared spectroscopy (IRAS),[8, 13] but more definitive interpretation requires simulated/reference spectra, and thus a knowledge of the atomic configuration around the active site.[17] Nevertheless, the charge state of the metal is frequently invoked to explain reactivity, although this is not without controversy; the cationic nature of Pt_1 has been linked to both stronger[8] and weaker[15] CO adsorption, with diametrically opposite conclusions regarding CO oxidation activity.

In this paper, we combine temperature-programmed desorption (TPD), XPS, scanning tunneling microscopy (STM), and DFT calculations to study CO adsorption on a series of model single atom catalysts; Cu_1, Ag_1, Au_1, Ni_1, Pd_1, Pt_1, Rh_1, and Ir_1 atoms on Fe_3O_4(001). Upon deposition at room temperature, all the metals assume the same 2-fold coordination to surface oxygen, allowing for

direct comparison. CO was selected as the probe molecule due to the abundance of experimental and computational results on metal surfaces and nanoparticles in the literature, and because many SAC studies focus on CO oxidation and the water gas shift reaction, where CO is a reactant. Moreover, the stretching frequency of adsorbed CO is typically used to probe the charge state of the metal in SAC systems,[8, 13, 17, 18] which makes a detailed understanding of the metal-CO interaction important.

Our results show that the CO binding strength broadly follows the trends established for the corresponding low index metal surfaces, i.e. group 11 < 10 < 9, but that significant differences emerge within the groups. Our DFT+U calculations reproduce the experimental data well, and show the trends are linked to both the electronic structure of the adatom, and to adsorbate-induced structural relaxations of the system. The combination of the two effects differs from metal to metal because each responds differently to the 2-fold coordination environment, and because each has a different relative affinity for CO and O. Where the agreement between experiment and theory is imperfect, we show that the catalyst structure evolves during the experiment. Ultimately, our results show that the behavior of SACs is better rationalized by analogy to coordination complexes rather than metal nanoparticles, and crucially, that the reactivity of the metal atoms in SAC can be tuned if the coordination environment can be controlled.

CO Adsorption Energies Determined by Experiment

The experiments described here were performed on several natural $Fe_3O_4(001)$ single crystals over a period of four years. The samples were prepared in ultrahigh vacuum (UHV) by cycles of Ar^+ or Ne^+ sputtering and 900 K annealing. The resulting surface exhibits the $(\sqrt{2}\times\sqrt{2})R45°$ LEED pattern and STM signature characteristic of the so-called subsurface cation vacancy (SCV) reconstruction,[19, 20] which is known to stabilize dense arrays of metal atoms to temperatures as high as 700 K.[20, 21] Metal is evaporated directly onto the as-prepared $Fe_3O_4(001)$ support in UHV (i.e. no additional ligands are present), and we define coverages in monolayers (ML, which corresponds to 1 atom per $(\sqrt{2}\times\sqrt{2})R45°$ unit cell, or 1.42×10^{14} per cm^2). In Fig. 1A, we show that Cu, Ag, Au, Ni, Pd, Pt, Rh, and Ir atoms all adsorb at the same location midway between the underlying rows of surface Fe atoms. Note that the surface oxygen atoms are not imaged in STM because they have no electronic states in the vicinity of the Fermi level, but their position is well known from quantitative electron [19] and x-ray diffraction [22] measurements and DFT-based calculations. The as-

deposited structure and thermal stability of the adatom systems shown in Fig. 1A have all been thoroughly characterized previously,[21, 23, 24, 25, 26, 27, 28, 29, 30] which makes this an ideal model system to systematically compare the adatom properties. The adsorption site is 2-fold coordinated to the surface oxygen atoms that do not have a subsurface tetrahedral Fe neighbor (Cu is shown as an example in Fig. 1B), which is essentially where the next Fe cation would reside if the bulk structure were continued outward. The height of the adatoms above the surface (z) varies significantly, however, and we recently measured this parameter for Cu, Ag, and Ni,[27, 28] and used the data to benchmark our theoretical approach. In Fig. 1A, all calculations are based on the optimal DFT+U approach (U_{eff} = 3.61 eV, optB88-DF functional)[27, 28].

Based on the current calculations, we find that all of the metal adatoms are cationic with charges in the range 0.28-0.68e (calculated as nominal valence – Bader charge). Ag, Au, and Pd are bound weakest (E_{ad} = -2.75 eV, -2.90 eV, and -2.99 eV, respectively), while Ir shows the strongest interaction (E_{ad} = -5.26 eV). Cu, Ni, Pt, and Rh lie in the range of -3.98 eV to -4.60 eV. Thus, the binding energy scales somewhat with the oxophilicity of the metal, in line with previous reports for oxide-supported metal clusters[31] and SACs,[32] although Pt is anomalously strong. Finally, we note that Ni,[25] Rh,[30] and Ir[29] adatoms are ultimately unstable against incorporation in the surface lattice, which is important in interpreting the TPD data presented in this paper.

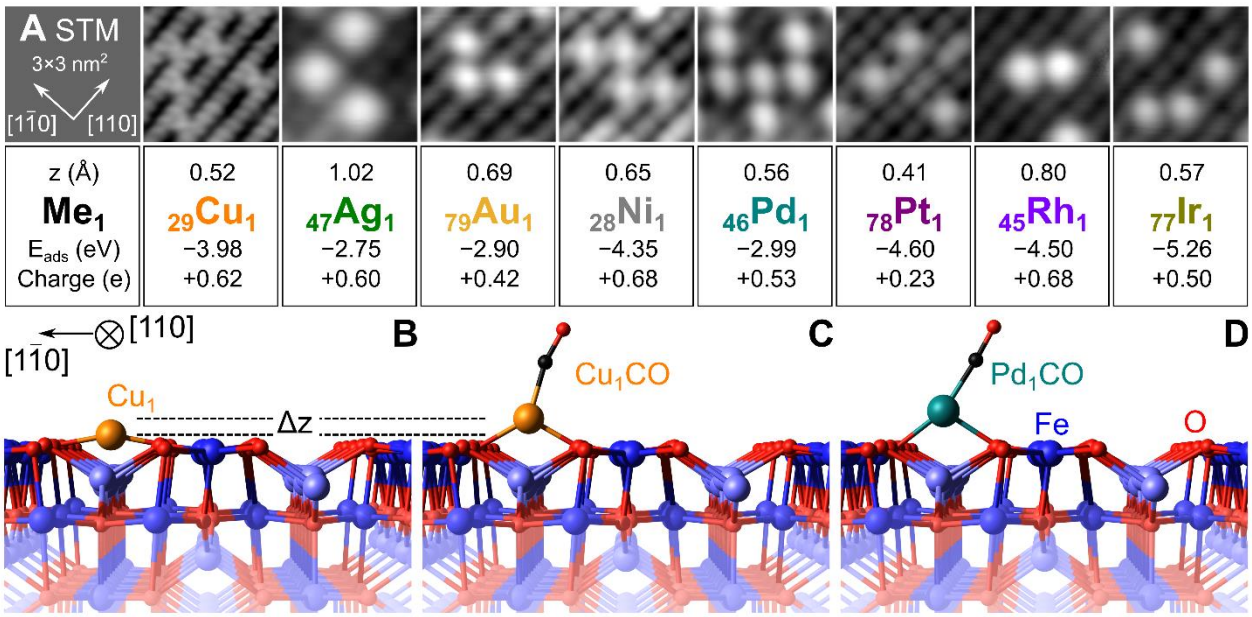

Figure 1: **Characterization of the Fe_3O_4(001)-based SAC model system.** (A) Representative STM images (3×3) nm², V_{sample} + 1-1.5 V, I_{tunnel} = 0.1-0.3 nA) showing metal adatoms adsorbed midway between the Fe

rows of the Fe_3O_4(001) support. Alongside each image are the DFT+U derived adsorption energies, nominal valence - Bader charge, and height of the adatom (*h*) above the surface Fe atoms in the 2-fold adsorption geometry. (B-D) DFT+U derived minimum energy structure for the Cu_1/Fe_3O_4(001) system (B) a Cu_1CO carbonyl (C), and a Pd_1CO carbonyl (D).

To determine how strongly CO binds to the different metal adatoms, we conducted a series of TPD experiments. We have shown previously[33] that CO interacts weakly with the Fe_3O_4(001) support, and desorbs from surface Fe^{3+} sites in two peaks between 60 K and 100 K (Fig. S1). Additional small desorption peaks between 100 K and 220 K arise due to CO desorbing from Fe^{2+} containing defects in the surface such as antiphase domain boundaries and step edges.[33] The grey curves shown in Figs. 2A-G show the "clean-surface" CO-TPD data acquired prior to adsorption of the metal adatoms (omitting the desorption peaks from the regular Fe sites, which is much larger, Fig. S1). Small differences exist in the relative intensity of the different defect peaks from experiment to experiment because these data were acquired using several different Fe_3O_4(001) samples.

The colored curves show selected CO-TPD data obtained after adsorption of metal adatoms at 300 K. In each case, the sample was cooled to 100 K, CO was adsorbed, and the sample heated with a 1 K/s ramp. An arrow marks the TPD peak corresponding to desorption of CO from the metal adatom in each case. The peak assignments are themselves the result of a series of STM, XPS and TPD experiments for different adatom coverages and experimental conditions. This is necessary because the Me_1/Fe_3O_4(001) systems are not static, and evolve differently to CO exposure and heating. In what follows, we briefly summarize the basis of the assignment for each metal. Further details can be found in the Supporting Information, and an exhaustive account of these experiments is contained within the PhD thesis of Hulva.[34]

Ag and Cu are particularly straightforward to interpret because STM measurements show the adatom phase is stable for coverages up to 0.5 ML. Moreover, the adatom arrays are thermally stable to temperatures as high as 700 K,[24] and following exposure to CO. Generally speaking, CO adsorption induces a positive core level shift in the XPS peaks associated with the adatom (Fig. S2), which disappears when the CO desorbs from the adatom. Naturally, the peak in C1s due to the adsorbed CO vanishes (Fig. S3). For both Cu and Ag, a small shoulder exists on the high temperature side of the main TPD peak. This results from a fraction of adatoms occupying a metastable geometry following room temperature deposition, and can be reduced in intensity by annealing the system prior to CO adsorption (See Figs. S4 and S5). For Cu, an additional sharp

peak is observed at 120 K. This may be due to the incorporation of Cu in the subsurface layers (the peak is close to that associated with Fe^{2+} defects in the clean surface on some samples), or the possibly the presence of $Cu(CO)_2$ dicarbonyls, which can be stabilized at low temperature according to our DFT+U calculations (Table S1).

Au was the most difficult system studied here because clusters coexist with adatoms already at very low coverages (>0.15 ML[21]), and because two CO TPD peaks grow together at 345 K and 300 K as the Au coverage is increased (Fig. S6). This suggests two inequivalent sites for adsorption. We assign the peak at 300 K to CO desorbing from regular Au adatoms because pre-annealing the system prior to CO adsorption increases the intensity of this peak relative to the 345 K peak, and because the 345 K peak intensity increases following exposure to water. This suggests the 345 K peak is probably related to Au adatoms interacting with surface hydroxyl groups (as has been observed previously by STM for Pd adatoms on this surface).[23]

Turning to the group 10 metals, the Ni peak at 300 K is straightforward to assign based on the CO-induced core level shift. The additional peak at 200 K may be related to Ni incorporated in the surface, as Ni is known to incorporate in the subsurface already at room temperature.[28] TPD data for Pd is not shown because CO adsorption destabilizes the adatoms leading to rapid agglomeration.[23] A similar process occurs for Pt,[26] but the TPD data remains interesting because CO exposure leads primarily to stable Pt_2 dimers.[26] The CO desorption peaks from Rh and Ir adatoms are again straightforward to assign, although these metals incorporate into the oxide lattice when the CO desorbs. Thus, the post desorption XPS peak exhibits a higher binding energy than the initial 2-fold adatom,[29] rather than shifting back to the as-deposited position. The data acquired at 0.1 ML Rh coverage is shown because this metal exhibits a lower temperature desorption peak for coverages above 0.2 ML.

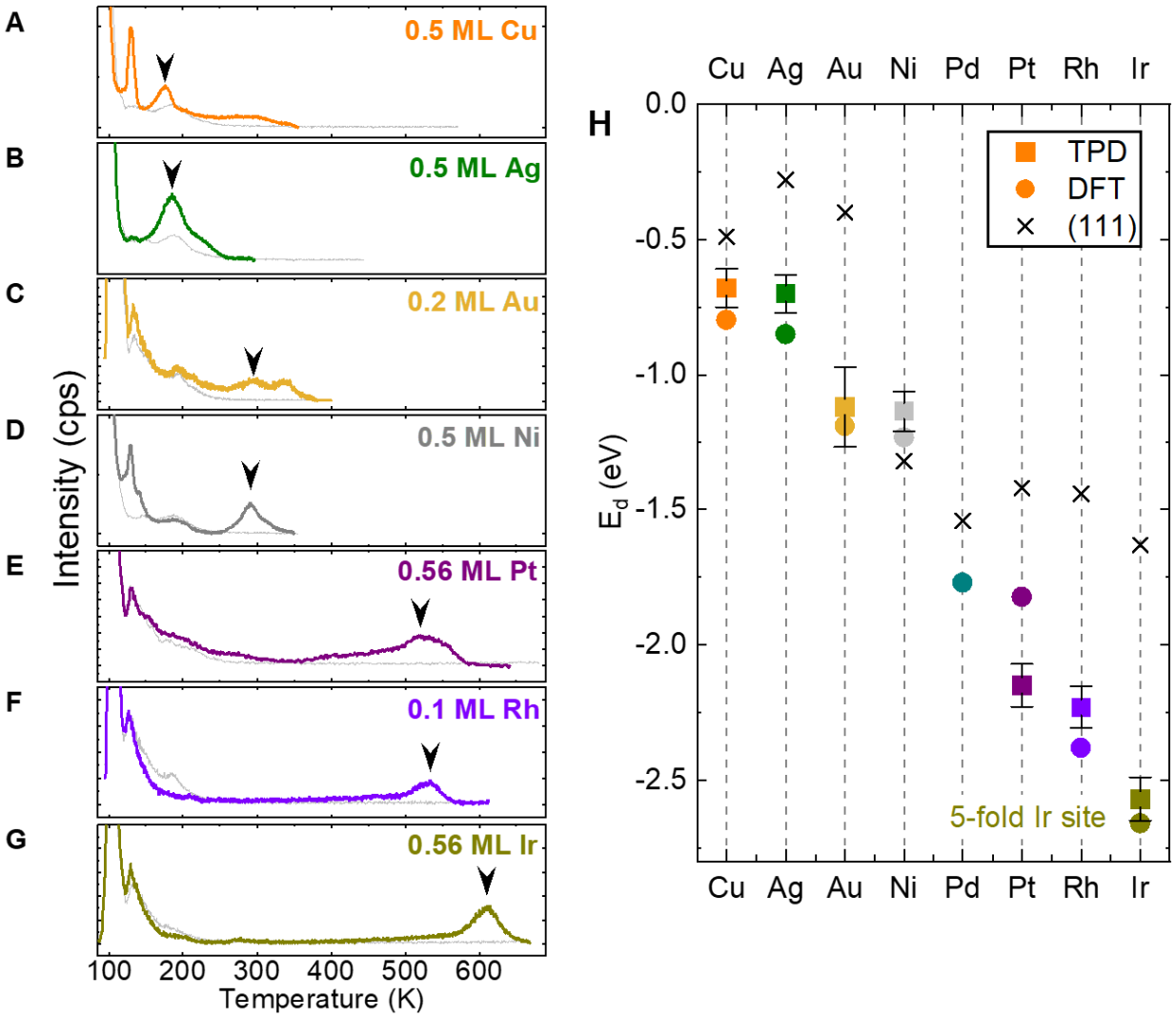

Figure 2: (A-G) CO TPD curves for various adatoms (1 ML corresponds to 1 metal atom per surface unit cell, or 1.42×10^{14} atoms per cm^2). (H) Plot of experimental and calculated CO adsorption/desorption energies, alongside experimental values for respective (111) surfaces. Error bars for the experimental data are calculated for the temperature uncertainty of ± 10 K (± 20 K for Au). E_d(eV) values for the (111) metal surfaces are taken from Ref. 35.

In Figure 2H, we convert the TPD peak temperatures into desorption energies (filled squares) using the Redhead equation.[36] While many TPD studies utilize a prefactor of 10^{13} s^{-1}, which corresponds to a molecule adsorbed in a corrugation-free surface potential, we assume that the molecule is highly constrained at the adatom site prior to adsorption, and has zero entropy. Then, the prefactor is given by $\nu = \frac{k_B T}{h} exp\left(\frac{\Delta S^{\#}}{k_B}\right)$, and $\Delta S^{\#}$ is simply the gas phase entropy minus the translational

degree of freedom perpendicular to the surface,[37] and the calculated desorption energies represent an upper limit.

The × symbols in Figure 2H show experimental desorption energies for the corresponding (111) metal surfaces obtained from Table 1 in ref 38. The basic trend is similar to the adatoms studied here (i.e. group 11 < group 10 < group 9), but there are large differences in the absolute magnitudes and the trends within groups also differ. Figure 2H also contains the PBE+U determined adsorption energies for a single CO molecule adsorbed on the metal adatoms (filled circles, also see Table S1). The DFT calculations track the experimental trend with a positive offset of ≈+0.2 eV for all metals (other than Pt, which forms dimers), which shows that the optB88-DF functional systematically overbinds the CO molecule (as suggested previously for water).[39] Nevertheless, the agreement is excellent, which gives us confidence to delve into the details of the calculations and understand how the "single atom" nature of the systems affects CO binding.

Trends Analyzed by Density Functional Theory

The d-band center of mass (d-COM) and the d-band filling are well-known descriptors affecting the CO adsorption energy on metals.[1, 40] Since both parameters change when the metal atoms become cationic and bind to oxygen, the CO adsorption energy will also be different. To investigate how the electronic structure of the metal site affects the CO binding, we performed an extensive set of calculations, where we compared CO adsorption on the $Me_1/Fe_3O_4(001)$ systems with (i) CO in atop sites on the corresponding (111) metal surfaces and (ii) on surface cation sites at the most stable facets of the respective metal oxide. The full dataset, all acquired using the same computational setup, is shown and discussed in the Supporting Information. In the following section we select 4 metals, Ni, Ag, Cu, and Ir, which allow to illustrate the most important factors involved. The position of the d-COM and oxidation state indeed play an important role, but we also identify the $O_{surface}$-Me_1-CO bond angle as an important factor. Distortions that result from the system attempting to achieve an ideal 180° bond angle can severely reduce the CO adsorption energy encountered in SAC systems, and the extent of these is shown to depend on the relative affinity of the metal to CO and O.

At first glance, one might guess that the oxide-supported metal adatoms considered here would be somewhat between a metal and an oxide, since they have a lower coordination than they would have in a stable metal oxide surface, and an intermediate oxidation state. However, Ni is the only

metal to exhibit such simple behavior (Fig. 3A). In this case, the nominal valence - Bader charge of the $Ni_1/Fe_3O_4(001)$ adatom (+0.68e) lies between that of a Ni atom in the metal (+0.01e) and NiO(100) (+1.19e) surfaces, suggestive of a +1 oxidation state. This configuration is not common in nature, but neither is a Ni geometry with 2-fold coordination to oxygen. For comparison, the Ni atoms in the NiO(100) surface are 5-fold coordinated and nominally 2+. This immediately shows that metastable geometries accessible in SAC can yield unique properties not found elsewhere. In Figure 3a, we plot the CO adsorption energy (E_{ads}(CO)) as a function of d-COM for these different systems, and see that the Ni_1 adatom lies between the metal and the oxide: as the Ni becomes more oxidized, the d-band moves further below E_F, and the CO binding weakens. While the adatom is lifted slightly away from the surface by CO adsorption, the effect is small compared to some of the other metals (Fig. 1). When a Ni atom replaces a 5-fold coordinated Fe at the $Fe_3O_4(001)$ surface, as has been found to occur in experiment,[41] the d-COM and E_{ads}(CO) are very similar to NiO(100) due to the similar coordination environment. At NiO(100), the large shift in d-COM away from E_F reduces back-donation to such an extent than the bond is primarily electrostatic in nature.[42]

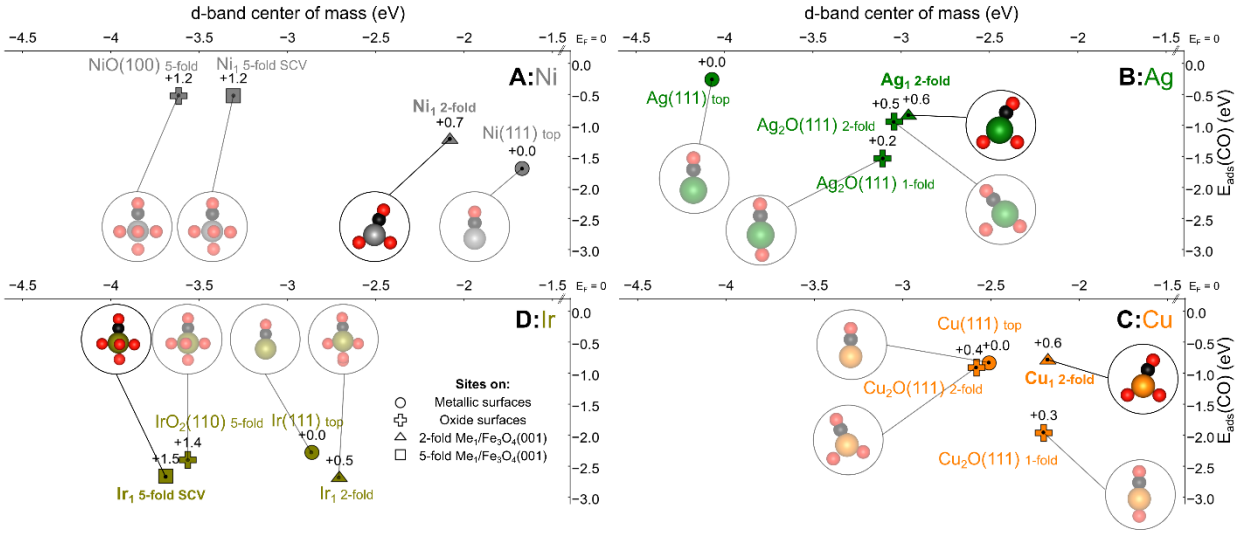

Figure 3: Comparison of CO adsorption energy for $Me_1/Fe_3O_4(001)$ SACs in comparison with Me(111) and MeO_x oxide surfaces. Adsorption energies are plotted against the d-band center of mass (d-COM) and indicated in each panel are the local adsorption configurations and the oxidation state (nominal valence - Bader charge) of the metal atom. (A) Nickel - As the oxidation state increases, the d-COM moves away from E_F and the CO binding energy decreases. Ni incorporated into a 5-fold site on $Fe_3O_4(001)$ is close to NiO(100) due to the similar bonding environment. (B) Silver - Oxidized Ag has its d-COM shifted

towards E_F leading to a stronger CO binding energy as compared to the metal. The 1-fold coordinated Ag atom on $Ag_2O(111)$ exhibits the strongest $E_{ads}(CO)$ due to a linear $O_{surface}$-Ag-CO geometry, the distorted geometries for 2-fold coordinated Ag at $Ag_2O(111)$ and $Ag_1/Fe_3O_4(001)$ are similar. (C) Copper – $E_{ads}(CO)$ for $Cu_1/Fe_3O_4(001)$ is similar to the Cu(111) surface despite a significant shift of d-COM towards E_F because energy is lost due to distortions of the adatom geometry (see Fig. 1). The 1-fold geometry on $Cu_2O(111)$ has no such distortions, and a significantly larger $E_{ads}(CO)$ due to its higher d-COM. (D) Iridium – the $E_{ads}(CO)$ at $Ir_1/Fe_3O_4(001)$ is enhanced over Ir(111) due to the formation of an additional bond to the subsurface oxygen atom, which creates a pseudo-square planar environment for the Ir adatom. Ir incorporated in the 5-fold geometry on $Fe_3O_4(001)$ behaves very much like a 5-fold coordinated atom in the $IrO_2(110)$ surface. Models show the first coordination sphere of the Me atom only with oxygen red, and carbon black.

Next, we tackle the noble metals Ag (Fig. 3B) and Cu (Fig. 3C), which exhibit a similar CO adsorption energy at the $Me_1/Fe_3O_4(001)$ adatom sites. This is in stark contrast to the respective (111) metal surfaces, which bind CO significantly stronger (Fig. 2G). It is straightforward to assign a +1 oxidation state to the Ag_1/Fe_3O_4 and Cu_1/Fe_3O_4 adatom configurations by analogy to the native Ag_2O and Cu_2O oxides,[27] which also have 2-fold coordination to oxygen. The nominal valence - Bader charge is similar to those found for 2-fold coordinated cations in the $Cu_2O(111)$ and $Ag_2O(111)$ surfaces and bulk. Since these metals give away the s-electron in the 1+ state, the d-shell is full and the interaction with CO is dominated by d-$2\pi^*$ back donation. Looking first at Ag, we calculate a much stronger CO binding energy at the Ag_1/Fe_3O_4 adatom (-0.85 eV) than on the Ag(111) surface (-0.26 eV), which we attribute to the large shift (+1.1 eV) in the d-COM towards E_F. Interestingly, both the 1-fold and 2-fold Ag atoms exposed at the $Ag_2O(111)$ surface have a similar d-COM to $Ag_1/Fe_3O_4(001)$, but the adsorption energy at the 1-fold site is significantly larger (-1.53 eV). Analyzing the structures before and after CO adsorption, we note that the 1-fold site (see fig. 3B) facilitates a favorable linear $O_{surface}$-Ag_1-CO geometry, whereas at the 2-fold site, a distortion occurs that results in partial weakening of the Ag-O surface bonds. This happens until an overall energetic equilibrium is reached, which is usually well short of the ideal 180° $O_{surface}$-Me-CO bond angle found at the 1-fold site. Crucially, the energetic cost of the substrate distortion required to accommodate the CO diminishes the total energy of the system, resulting in a reduced adsorption energy of -0.94 eV. The $Ag_1/Fe_3O_4(001)$, with its 2-fold coordination shows a similar distortion. Thus, the adsorption configuration also plays a role.

In the case of Cu, the Cu_1-CO bond is strengthened with respect to the metal (111) surface as d-COM shifts closer to E_F, which is visible in the shorter Cu-C bond length (1.81 Å vs. 1.86 Å). However, the large distortion to the adatom geometry that occurs upon CO adsorption (visible in Fig. 1) reduces the total energy such that it becomes almost the same as on the metal, where weaker binding, but little distortion occurs. Thus, the bond strengthening caused by the electronic structure is counteracted by the relaxations in the system. On $Cu_2O(111)$, the 1-fold site has a d-COM shifted towards E_F, and since no distortion is required to bind the CO favorably, $E_{ads}(CO)$ is significantly stronger (-1.96 eV). In general, the extent of the distortion observed for each metal adatom is related to the relative affinity of that metal to bind CO or the oxide. In Fig. S8a, we plot the binding energy calculated for O and CO to a gas phase atom. As the reactivity of the metal surface increases from Ag, to Ni, to Rh and Ir, the binding to CO and O increases in proportion to one another. Pd and Pt, however, are outliers and clearly exhibit a preference for CO, explaining why these metals are lifted the most, and sinter in the experiments.

Next, we consider Ir (Fig. 3D), which bears many similarities to Rh. Both have a partially filled d-band, and thus a much larger 5σ-d donation contribution to the CO binding.[35] The oxidation of the Ir adatom in the 2-fold SAC adatom geometry reduces the d-band filling still further, which enhances the interaction with CO. Also, the preference for Ir to form a square-planar geometry in the 1+ oxidation state induces the Ir adatom to form an additional bond to a subsurface O atom, as discussed previously. In any case, desorption ultimately occurs from a 5-fold Ir atom in the TPD experiment, and this site has increased oxidation relative to the 2-fold adatom. This further reduces the d-filling, promotes the 5σ-d donation from the molecule, and strengthens the bond. Interestingly, in this case the low d-COM (-3.69 eV below E_F) reduces the split to the 5σ orbital, and the combination of these effects makes the 5-fold Ir site exhibit the strongest CO adsorption energy observed in our work.

Finally, we briefly discuss dicarbonyls. We have shown previously that 2-fold Ir forms dicarbonyl species due to its preference for a square planar Ir(I) geometry.[29] Interestingly, our calculations show that Ir is the only adatom where a dicarbonyl is thermodynamically favorable, i.e., the addition of a second CO is more favorable than the first (See Table S2). Nevertheless, dicarbonyls can be formed on almost all metals considered here, and the energetics and CO chemical potential will define the extent of dicarbonyl formation on a case by case basis. The current calculations

confirm that dicarbonyls cannot be formed at any 5-fold site coordinated adatom site, as shown previously for Ir.[29]

Overall, we conclude that knowledge of the local geometry is essential to understand the adsorption properties of supported metal adatoms. No simple trends are observed moving from metal to metal across the periodic table, and the observed properties stem directly from the electronic structure of the metal and its relative affinity for O and CO. Often, the adsorption energy is reduced relative to the d-band position because the structure is distorted when the system tries to adopt a 180° $O_{surface}$-Me_1-CO bond angle. The significant sensitivity on coordination and bond angles clearly demonstrate that single atom catalysts should not as the smallest possible supported nanoparticles, and that such systems are better viewed as undercoordinated coordination complexes. This has important consequences for the choice of metal in SAC design, and it is not necessarily the case that the best supported-metal nanoparticle catalyst will be the best SAC for a particular reaction.

Acknowledgements

The authors would like to thank Paul T. P. Ryan (Imperial College) for useful discussions. GSP, JH, MM, ZJ and RB acknowledge funding from the Austrian Science Foundation (FWF) Start Prize Y847-N20, and UD acknowledges the Austrian Science Fund FWF (Project 'Wittgenstein Prize, Z250-N27). GSP and MM acknowledge funding from the European Research Council (ERC) under the European Union's HORIZON2020 Research and Innovation program (ERC Grant Agreement No. [864628]. ZJ also acknowledges support from the TU Wien Doctoral Colleges TU-D. The computational results were achieved in part using the Vienna Scientific Cluster (VSC 3 and VSC 4).

References

1. Hammer B, Morikawa Y, Norskov JK. CO chemisorption at metal surfaces and overlayers. *Phys Rev Lett* 1996, **76**(12)**:** 2141-2144.

2. Yang XF, Wang A, Qiao B, Li J, Liu J, Zhang T. Single-atom catalysts: a new frontier in heterogeneous catalysis. *Acc Chem Res* 2013(8)**:** 1740-1748.

3. Liang S, Hao C, Shi Y. The power of single-atom catalysis. *ChemCatChem* 2015, **7**(17)**:** 2559-2567.

4. Liu J. Catalysis by supported single metal atoms. *ACS Catal* 2016, **7**(1)**:** 34-59.

5. Gates BC, Flytzani-Stephanopoulos M, Dixon DA, Katz A. Atomically dispersed supported metal catalysts: perspectives and suggestions for future research. *Catal Sci Technol* 2017, **7**(19)**:** 4259-4275.

6. Wang A, Li J, Zhang T. Heterogeneous single-atom catalysis. *Nat Rev Chem* 2018, **2**(6)**:** 65-81.

7. Zhang H, Liu G, Shi L, Ye J. Single-atom catalysts: Emerging multifunctional materials in heterogeneous catalysis. *Adv Energy Mater* 2018, **8**(1)**:** 1701343.

8. Ding K, Gulec A, Johnson AM, Schweitzer NM, Stucky GD, Marks LD, *et al.* Identification of active sites in CO oxidation and water-gas shift over supported Pt catalysts. *Science* 2015, **350**(6257)**:** 189-192.

9. Chen F, Jiang X, Zhang L, Lang R, Qiao B. Single-atom catalysis: Bridging the homo- and heterogeneous catalysis. *Chinese J Catal* 2018, **39**(5)**:** 893-898.

10. Cui X, Li W, Ryabchuk P, Junge K, Beller M. Bridging homogeneous and heterogeneous catalysis by heterogeneous single-metal-site catalysts. *Nat Catal* 2018, **1**(6)**:** 385-397.

11. Lang R, Li T, Matsumura D, Miao S, Ren Y, Cui Y-T, *et al.* Hydroformylation of olefins by a rhodium single-atom catalyst with activity comparable to $RhCl(PPh_3)_3$. *Angew Chem Int Ed* 2016, **55**(52)**:** 16054-16058.

12. Liu J. Aberration-corrected scanning transmission electron microscopy in single-atom catalysis: Probing the catalytically active centers. *Chinese J Catal* 2017, **38**(9)**:** 1460-1472.

13. Thang HV, Pacchioni G, DeRita L, Christopher P. Nature of stable single atom Pt catalysts dispersed on anatase TiO_2. *J Catal* 2018, **367:** 104-114.

14. Liang J, Yu Q, Yang X, Zhang T, Li J. A systematic theoretical study on FeO_x-supported single-atom catalysts: M_1/FeO_x for CO oxidation. *Nano Res* 2018, **11**(3)**:** 1599-1611.

15. Qiao B, Wang A, Yang X, Allard LF, Jiang Z, Cui Y, *et al.* Single-atom catalysis of CO oxidation using Pt_1/FeO_x. *Nat Chem* 2011, **3**(8)**:** 634-641.

16. Li F, Li Y, Zeng XC, Chen Z. Exploration of high-performance single-atom catalysts on support M_1/FeO_x for CO oxidation via computational study. *ACS Catal* 2014, **5**(2)**:** 544-552.

17. DeRita L, Resasco J, Dai S, Boubnov A, Thang HV, Hoffman AS, *et al.* Structural evolution of atomically dispersed Pt catalysts dictates reactivity. *Nat Mater* 2019.

18. Resasco J, Dai S, Graham G, Pan X, Christopher P. Combining in-situ transmission electron microscopy and infrared spectroscopy for understanding dynamic and atomic-scale features of supported metal catalysts. *J Phys Chem C* 2018.

19. Bliem R, McDermott E, Ferstl P, Setvin M, Gamba O, Pavelec J, *et al.* Subsurface cation vacancy stabilization of the magnetite (001) surface. *Science* 2014, **346**(6214)**:** 1215-1218.

20. Parkinson GS. Iron oxide surfaces. *Surf Sci Rep* 2016, **71**(1)**:** 272-365.

21. Novotny Z, Argentero G, Wang Z, Schmid M, Diebold U, Parkinson GS. Ordered array of single adatoms with remarkable thermal stability: $Au/Fe_3O_4(001)$. *Phys Rev Lett* 2012, **108**(21)**:** 216103.

22. Arndt B, Bliem R, Gamba O, van der Hoeven JES, Noei H, Diebold U, *et al.* Atomic structure and stability of magnetite $Fe_3O_4(001)$: An X-ray view. *Surf Sci* 2016, **653:** 76-81.

23. Parkinson GS, Novotny Z, Argentero G, Schmid M, Pavelec J, Kosak R, *et al.* Carbon monoxide-induced adatom sintering in a Pd-Fe_3O_4 model catalyst. *Nat Mater* 2013, **12**(8)**:** 724-728.

24. Bliem R, Kosak R, Perneczky L, Novotny Z, Gamba O, Fobes D, *et al.* Cluster nucleation and growth from a highly supersaturated adatom phase: silver on magnetite. *ACS Nano* 2014, **8**(7)**:** 7531-7537.

25. Bliem R, Pavelec J, Gamba O, McDermott E, Wang Z, Gerhold S, *et al.* Adsorption and incorporation of transition metals at the magnetite Fe_3O_4(001) surface. *Phys Rev B* 2015, **92**(7)**:** 075440.

26. Bliem R, van der Hoeven JE, Hulva J, Pavelec J, Gamba O, de Jongh PE, *et al.* Dual role of CO in the stability of subnano Pt clusters at the $Fe_3O_4$001) surface. *Proc Natl Acad Sci USA* 2016, **113**(32)**:** 8921-8926.

27. Meier M, Jakub Z, Balajka J, Hulva J, Bliem R, Thakur PK, *et al.* Probing the geometry of copper and silver adatoms on magnetite: quantitative experiment versus theory. *Nanoscale* 2018, **10**(5)**:** 2226-2230.

28. Ryan PTP, Jakub Z, Balajka J, Hulva J, Meier M, Kuchle JT, *et al.* Direct measurement of Ni incorporation into Fe_3O_4(001). *Phys Chem Chem Phys* 2018, **20**(24)**:** 16469-16476.

29. Jakub Z, Hulva J, Meier M, Bliem R, Kraushofer F, Setvin M, *et al.* Local Structure and Coordination Define Adsorption in a Model Ir1/Fe3O4 Single-Atom Catalyst. *Angew Chem Int Ed* 2019, **58**(39)**:** 13961-13968.

30. Jakub Z, Hulva J, Ryan PTP, Duncan DA, Payne DJ, Bliem R, *et al.* Adsorbate-induced structural evolution changes the mechanism of CO oxidation on a Rh/Fe3O4(001) model catalyst. *Nanoscale* 2020, **12**(10)**:** 5866-5875.

31. Hemmingson SL, Campbell CT. Trends in adhesion energies of metal nanoparticles on oxide surfaces: Understanding support effects in catalysis and nanotechnology. *ACS Nano* 2017, **11**(2)**:** 1196-1203.

32. O'Connor NJ, Jonayat ASM, Janik MJ, Senftle TP. Interaction trends between single metal atoms and oxide supports identified with density functional theory and statistical learning. *Nat Catal* 2018, **1**(7)**:** 531-539.

33. Hulva J, Jakub Z, Novotny Z, Johansson N, Knudsen J, Schnadt J, *et al.* Adsorption of CO on the Fe_3O_4(001) surface. *J Phys Chem B* 2018, **122**(2)**:** 721-729.

34. Hulva J. Studies of adsorption on Fe3O4(001) using molecular beams. PhD thesis, TU Wien, 2019.

35. Koper MTM, Santen RAv, Wasileski SA, Weaver MJ. Field-dependent chemisorption of carbon monoxide and nitric oxide on platinum-group (111) surfaces: Quantum chemical calculations compared with infrared spectroscopy at electrochemical and vacuum-based interfaces. *J Chem Phys* 2000, **113**(10)**:** 4392-4407.

36. Redhead PA. Thermal desorption of gases. *Vacuum* 1962, **12**(4)**:** 203-211.

37. Campbell CT, Sellers JRV. The Entropies of Adsorbed Molecules. *J Am Chem Soc* 2012, **134**(43)**:** 18109-18115.

38. Gajdoš M, Eichler A, Hafner J. CO adsorption on close-packed transition and noble metal surfaces: trends from *ab initio* calculations. *J Phys: Condens Matter* 2004, **16**(8)**:** 1141-1164.

39. Gillan MJ, Alfè D, Michaelides A. Perspective: How good is DFT for water? *J Chem Phys* 2016, **144**(13)**:** 130901.

40. Stroppa A, Kresse G. The shortcomings of semi-local and hybrid functionals: what we can learn from surface science studies. *New Journal of Physics* 2008, **10**(6)**:** 063020.

41. Jakub Z, Hulva J, Mirabella F, Kraushofer F, Meier M, Bliem R, *et al.* Nickel Doping Enhances the Reactivity of Fe3O4(001) to Water. *J Phys Chem C* 2019, **123**(24)**:** 15038-15045.

42. Pacchioni G, Valentin CD, Dominguez-Ariza D, Illas F, Bredow T, Klüner T, *et al.* Bonding of NH3, CO, and NO to NiO and Ni-doped MgO: a problem for density functional theory. *J Phys: Condens Matter* 2004, **16**(26)**:** S2497-S2507.